Nanoscale

PAPER

View Article Online
View Journal

Cite this: DOI: 10.1039/c4nr01105h

A novel biosensor for quantitative monitoring of on-target activity of paclitaxel†

H. E. Townley,‡[a,b] Y. Zheng,‡[b,c] J. Goldsmith,[b,c] Y. Y. Zheng,[b,c] M. R. L. Stratford,[d] P. J. Dobson[a] and A. A. Ahmed*[b,c]

This study describes a system for quantifying paclitaxel activity using the C-terminus of α-tubulin as a biomarker. Following stabilization of microtubules with paclitaxel, a specific detyrosination reaction occurs at the C-terminus of α-tubulin which could be used to assess efficacy. A fluorescence resonance energy transfer (FRET) based biosensor was synthesized comprising a short peptide that corresponded to the C-terminus of α-tubulin, a fluorophore (Abz), and a quencher (Dnp). The fluorophore added to the end of the peptide can be released upon enzymatic detyrosination. In addition, a single fluorophore-tagged peptide was also conjugated to mesoporous silica nanoparticles to examine the feasibility of combining the drug with the peptide biomarker. As a proof of concept, we found that the degree of peptide cleavage, and therefore enzymatic activity, was directly correlated with exogenous bovine carboxypeptidase (CPA) an enzyme that mimics endogenous detyrosination. In addition, we show that cell lysates obtained from paclitaxel-treated cancer cells competed with exogenous CPA for biosensor cleavage in a paclitaxel dose-dependent manner. Our work provides strong evidence for the feasibility of combining paclitaxel with a novel biosensor in a multi-load nanoparticle.

Received 27th February 2014,
Accepted 8th November 2014

DOI: 10.1039/c4nr01105h

www.rsc.org/nanoscale

Introduction

Paclitaxel is licensed for the treatment of many solid malignancies including ovarian and breast cancer. Paclitaxel binds to a specific pocket that resides in β-tubulin and this induces microtubule polymerization and stabilization, and failure of appropriate formation of a mitotic spindle. Since paclitaxel significantly increases the half-life of microtubules they become available for several posttranslational modifications including α-tubulin detyrosination by a tubulin-specific carboxypeptidase. The magnitude of these modifications is directly proportionate to the degree of drug-induced microtubule stabilisation.[1,2] Moreover, Ahmed *et al.*, have previously shown that α-tubulin detyrosination and paclitaxel-induced microtubule stabilisation directly correlate with baseline microtubule stability.[1,2] Thus, it is plausible to hypothesise that α-tubulin detyrosination could be used as a biomarker for measuring the efficacy of paclitaxel-induced microtubule stabilisation. Since paclitaxel elicits a response only in a fraction of tumours,[3] direct measurement of its on-target activity could provide a means to select patients for further treatment.

Paclitaxel has been used in doses ranging from 60–250 mg/m^{-2}, over 1–96 hours and from 1–3 weekly intervals.[4] This drug has a large inter-individual variation in pharmacokinetics with the AUCinf (area under the plasma concentration time curve from time zero extrapolated to the infinite time) having an average coefficient of variation (CV) in the range of 20–50%.[5–9] While it is known that hepatic impairment and obesity contribute to this discrepancy, the cause of the large variation is not well understood.[10] As such, even after two decades of clinical research, no ideal dosing strategy exists.[4] The use of a sensitive biosensor to monitor on-target activity could be utilized in the optimization of the drug dose while under treatment.

Paclitaxel has poor solubility and is, therefore, administered as a Cremophor EL, a polyoxyethylated castor oil, preparation. Many of the side effects of the drug, such as blood vessel inflammation at the administration site and hypersensitivity reactions are directly attributable to its formulation. Because of its poor solubility, higher drug doses are required to achieve therapeutic concentrations at the tumour site but at the expense of inducing dose-dependent side effects. The recent

[a]Department of Engineering Sciences, Parks Road, Oxford, OX1 3PJ, UK. E-mail: Helen.Townley@eng.ox.ac.uk, Peter.Dobson@eng.ox.ac.uk
[b]Nuffield Department of Obstetrics and Gynaecology, Women's Centre, John Radcliffe Hospital, Oxford, OX3 9DU, UK
[c]Weatherall Institute of Molecular Medicine, University of Oxford, Headington, Oxford, OX3 9DS, UK. E-mail: Juliet.Goldsmith@ucsf.edu, zyhk8@yahoo.com, Ahmed.Ahmed@obs-gyn.ox.ac.uk
[d]Department of Oncology, Old Road Campus Research Building, Roosevelt Drive, Oxford, OX3 7DQ, UK. E-mail: Michael.Stratford@oncology.ox.ac.uk
†Electronic supplementary information (ESI) available. See DOI: 10.1039/c4nr01105h
‡These authors have contributed equally.

introduction of novel paclitaxel formulations provides a strong proof-of-concept that enhancing the pharmacokinetics of paclitaxel is likely to improve it therapeutic efficacy.[11] Thus the use of a combination of novel nanoparticle paclitaxel formulations and a reliable biomarker of activity is likely to improve patient outcome.

Here we describe the synthesis and efficacy of a novel combination of a nanoparticle-based paclitaxel preparation and a biosensor for measuring the on-target activity of paclitaxel.

Results

Mesoporous silica nanoparticles as a carrier for paclitaxel

Mesoporous silica nanoparticles (MSNPs) were synthesized as a vehicle for delivering both the biosensor and the drug to cells. The physical parameters of these nanoparticles have been analysed in detail and previously presented.[12] The nanoparticles have an external size of 105.6 nm (±23.11 SD, n = 431) and internal pore channels that run through the length of the particle arranged in a quasi-hexagonal structure (Fig. 1). X-Ray diffraction (XRD) of the MSNPs is given as ESI.† The diameter of the pores was determined to be 2.13 nm (±0.21 SD, n = 544) by analysis of TEM images, and a similar result was given by Barret-Joyner-Halenda (BJH) analysis. Surface area analysis showed a very high surface area of the nanoparticles consistent with the removal of the template from the pores. Therefore, the external diameter of the MSNPs is of an appropriate size to be taken up by cells in a passive manner by endocytosis through the cell membrane. Furthermore, since the space-fill diagram of taxol has been shown to fit within a unit 1 × 1.5 × 2 nm,[13] it would be expected that paclitaxel could be loaded into the pores and channels of the MSNPs.

The uptake of the paclitaxel from solution into the pores of the MSNPs was assessed by mass spectrometry of the drug remaining in the supernatant after incubation with MSNPs. Uptake was found to be approximately 99%. Similarly high uptake rates were found with MSNPs and Ophiobolin.[14]

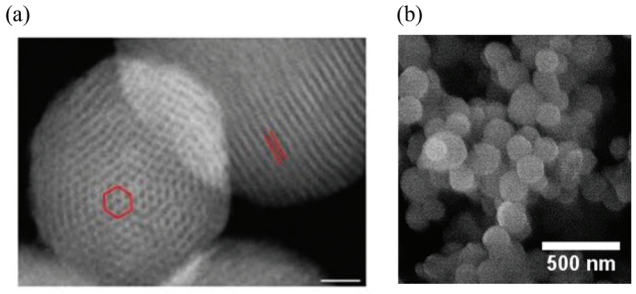

Fig. 1 Mesoporous silica nanoparticles. Electron microscopy images to show the morphology of the mesoporous silica nanoparticles. (a) Transmission electron microscopy (TEM) image; pores can be seen to display hexagonal symmetry when imaged normal to the beam, and channels (example highlighted by two parallel lines) can be seen in individual particles parallel to the beam. Scale bar; 10 nm. (b) Scanning electron microscopy (SEM) image; particles are roughly spherical in shape, and uniform in size.

To determine the efficacy of the novel drug-loaded nanoparticles, SKOv3 ovarian cancer cells were exposed to either paclitaxel-loaded nanoparticles or free paclitaxel at concentrations ranging from 0 to 200 nM, and incubated overnight. Cells were fixed and immunostained with anti-phospho histone H3 (P-histone H3), a specific marker for mitosis.[15] As expected, there was an upward trend in the percentage of cells staining positive for P-histone H3 with increasing paclitaxel concentrations (Fig. 2a, b). There was a statistically significant increase between 20 nM and 40 nM (P = 0.01), but no statistical increase between 40, 100 and 200 nM. The loaded nanoparticles induced a significant increase in mitotic arrest that was equivalent to

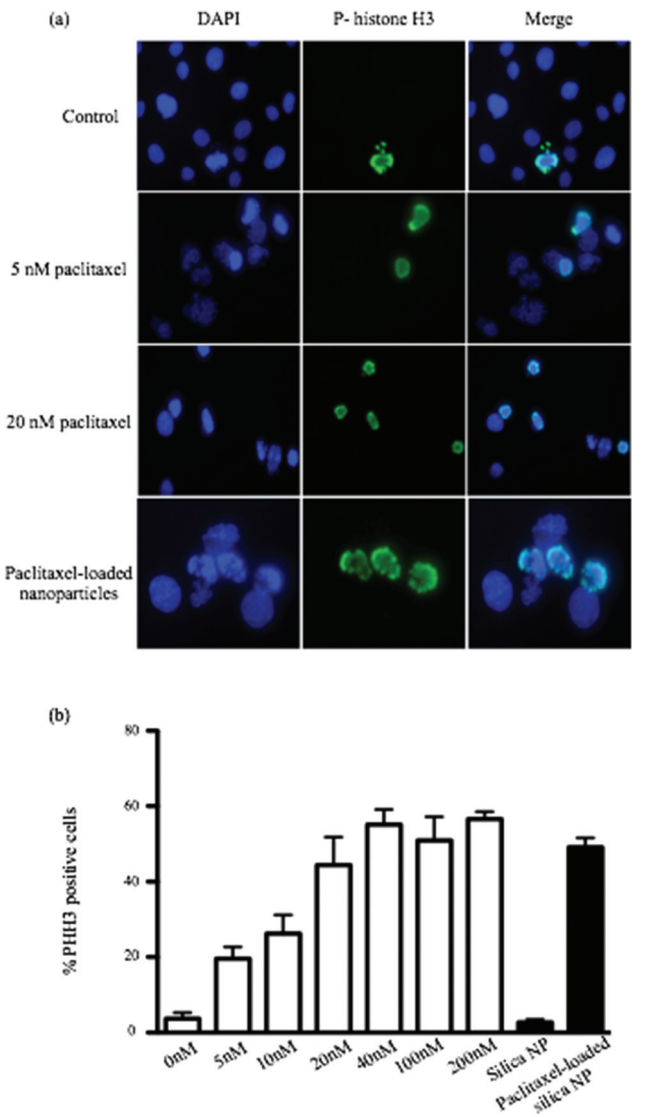

Fig. 2 Efficacy of paclitaxel-loaded particles in inducing mitotic arrest. (a) Cells were treated with 5 nM or 20 nM paclitaxel, or nanoparticles loaded with paclitaxel. Cells were immunostained with P-Histone H3 antibody, and the nucleus counterstained with DAPI, (b) Quantification of percentage of mitotic cells in the cell population after treatment with either paclitaxel at the indicated concentrations or paclitaxel (approx. 226 nM) loaded nanoparticles. PHH3; phospho Histone H3.

the highest concentration of free paclitaxel used. Importantly, empty mesoporous silica nanoparticles (MSNPs) did not induce mitotic arrest in SKOv3 cells (Fig. 2b). The above data confirmed the efficacy of the nanoparticles in culture.

Mesoporous silica nanoparticles as a carrier for a biosensor

We next tested the feasibility of the use of a cleavable peptide as a biosensor for paclitaxel activity. To do this, we synthesised a peptide that comprised the last eight amino acids of the human α-tubulin protein (GEEEGEEY). The N-terminus was modified by adding a FITC fluorogenic group, separated from the peptide by an aminohexanoic spacer. The C-terminus was modified by the addition of an amidated terminal lysine residue (Fig. 3). Since the silica surface of the nanoparticle has a high density of silanol groups it is particularly amenable to functionalization.[16] Thus, the nanoparticle surface was modified by SiO_2 amination with aminopropyltriethoxy silane (APTES) followed by conjugation of the peptide to the surface using a BS^3 amine-to-amine crosslinker *via* the primary amine of the lysine residue. The linker also incorporates an eight carbon spacer arm to prevent steric hindrance between the fluorophore and the peptide. Since the peptide was tethered to the particle, the feasibility of peptide cleavage could be tested by measuring free *versus* particle-bound fluorescence after exposure to a detyrosinase enzyme (Fig. 3).

Detyrosination of the peptide sequence would result in cleavage between the glutamic acid (E) and tyrosine (Y) residues, thereby releasing the fluorophore from the remainder of the particle bound peptide. A calibration curve was generated and it was seen that there was a consistent linear relationship between the peptide concentration and the fluorescence emission (data not shown) and therefore data has been expressed as change in fluorescence. In a typical conjugation reaction, 2 micromoles peptide are bound per g silica nanoparticles.

Cleavage of bound alpha-tubulin peptide is directly related to exogenous carboxypeptidase A (CPA) enzyme concentration. As a proof-of-concept, the nanoparticle–peptide construct was incubated with Bovine pancreatic carboxypeptidase A (Type II; Sigma) which is known to hydrolyze the peptide bonds of C-terminal residues with aromatic or aliphatic side chains. The bound peptide was incubated with CPA enzyme, the supernatant collected, and the fluorescence signal assessed. CPA induced a dose dependent increase in the fluorescence signal (CPA enzyme dose range: 0.1 U–0.3 U; Fig. 4).

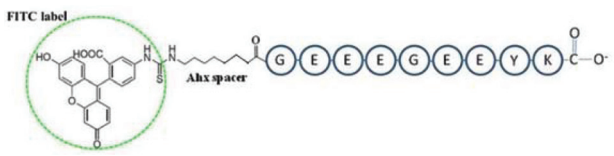

Fig. 3 Fluorescence peptide. Diagram to show the peptide comprising the C-terminal domain of alpha-tubulin with the addition of a FITC group at the N-terminus separated from the peptide by an aminohexanoic acid (Ahx) spacer.

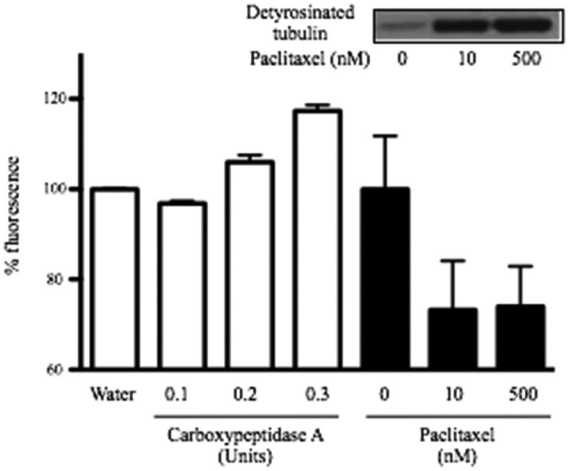

Fig. 4 Enzymatic cleavage of FITC-peptide sequence. The nanoparticle-bound peptide comprising the C-terminal end of alpha tubulin was incubated with either bovine CPA enzyme or cell lysates incubated with paclitaxel at 10 nM and 500 nM. Insert shows the result of a western blot of lysates probed with anti-detyrosinated tubulin antibody as a positive control for the effect of paclitaxel on microtubules. Water, and Cell lysate (0 nM) have been set to 100 percent.

Cleavage of bound alpha-tubulin peptide is inversely related to paclitaxel concentration in cell lysates. To ascertain the behaviour of the system on live cells, we prepared cell lysates from SKOv3 cells that were pre-incubated with paclitaxel. The lysates were probed with detyrosinated tubulin antibody (anti-Glu tubulin) and the amount of detyrosinated α-tubulin can be seen to increase when the cells were incubated with paclitaxel. Incubation of the nanoparticle–peptide with the cell lysates showed that cells which had not been incubated with paclitaxel were able to cleave the peptide, whereas cells incubated with paclitaxel showed lower fluorescence and therefore a decreased ability to cleave the peptide (Fig. 4). This suggested that there was substrate competition between the peptide and the endogenous paclitaxel-stabilised microtubules.

Biosensing using a FRET peptide

An extension of the concept shown in Fig. 3 is to use a FRET peptide. While the FITC-labelled peptide–nanoparticle construct described above would enable paclitaxel and the peptide to be delivered within a single carrier, the system requires separation of the supernatant to measure the enzymatic activity of the carboxypeptidase. While this provided a proof of concept *in vitro,* it can not be utilized in live cells. Thus, a FRET-based peptide in which a fluorescence signal would only be visible after peptide cleavage, was synthesised (Fig. 5). In addition to conjugation of the FRET peptide to a nanoparticle delivery system, the FRET peptide could also be used as an independent reporter molecule. We synthesised a peptide with an N-terminal 2-aminobenzoyl (Abz) group and a C-terminal 2,4-dinitrophenyl (Dnp) derivitized lysine (Fig. 5). We reasoned that the fluorescence of the N-terminal Abz group would be quenched in the intact peptide by the Dnp group through

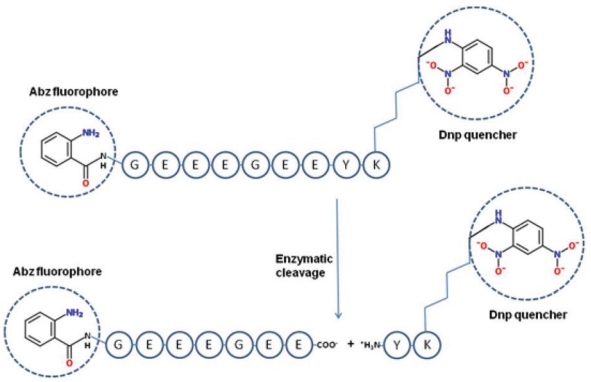

Fig. 5 Schematic representation of the FRET peptide. A peptide was synthesised comprising the C-terminal domain of alpha-tubulin with an Abz/Dnp donor/acceptor pair. Upon enzymatic cleavage of the tyrosine residue the fluorescence is released.

intramolecular resonance energy transfer. Peptide cleavage would relieve this intramolecular fluorescence quenching and result in increased fluorescence.

Indeed, the intact peptide showed a fluorescence peak at 520 nm (λ_{ex} 310 nm). Incubation with the proteolytic enzyme, CPA, cleaved the peptide, diminished the 520 nm peak, and induced a peak at approximately 414 nm, attributable to the released fluorescence from Abz (Fig. 6a).

In addition, the increased fluorescence strongly correlated with CPA treatment in a dose-dependent and time-dependent manner (Fig. 6b). As a control it was shown that there was no increase in fluorescence output when either buffer, enzyme or peptide were incubated in the absence of the other components. These results strongly suggest that the FRET-peptide could be used as a readout of the activity of CPA.

To test whether the peptide could be used as a readout of activity of endogenous tubulin-specific carboxypeptidase we used lysates that were obtained from SKOv3 cells that were pre-treated with increasing concentrations of paclitaxel as previously described. SKOv3 cells were incubated with paclitaxel at final concentrations of 0, 5, 10, 20, 40, and 100 nM. Incubation of the peptide with lysates from cells which had not been incubated with paclitaxel showed greater activity in cleaving the peptide than CPA. However, incubation with lysates from cells previously treated with increasing concentrations of paclitaxel induced a decrease in fluorescence (Fig. 7), similar to the results obtained using the particle-bound peptide. These results strongly suggest that the FRET-based assay could be used to measure endogenous carboxypeptidase activity.

Cell lysates from paclitaxel competitively inhibit CPA's ability to cleave the FRET peptide. To test the assumption of substrate competition between the FRET-based peptide and paclitaxel-treated microtubules, we conducted a further competition assay using CPA. Since CPA has been previously shown to induce detyrosination of microtubules,[17] we reasoned that pre-incubation of CPA with paclitaxel-treated cells would deplete CPA's activity and that this would be reflected on a decrease in CPA-mediated cleavage of the peptide biosensor.

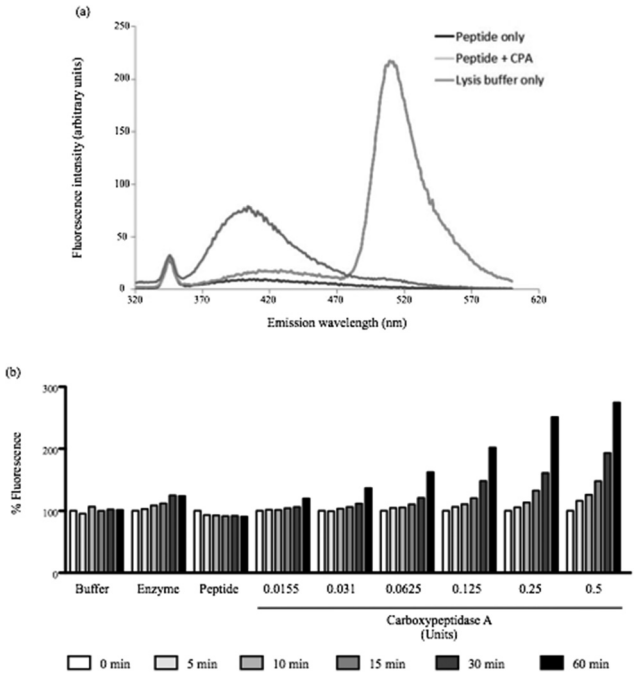

Fig. 6 Enzymatic cleavage of the FRET peptide with bovine CPA. (a) Spectrum showing fluorescence before and after incubation with CPA (b) time course to demonstrate the kinetics of peptide cleavage under varying enzyme concentrations. Columns labelled Buffer, enzyme and peptide contain only one component. Columns labelled with the number of enzyme units in the assay comprise all components.

Therefore, cell lysates from SKOv3 cells that were pre-incubated with concentrations of paclitaxel ranging from 0–100 nM were then incubated with 0.5 U CPA for 1 hour. Note that only a small dose was chosen to make the effect of depletion of CPA activity clearer. Subsequently, the FRET peptide was added for 1 hour prior to assessment of cleavage. The fluorescence signal decreased in the lysates from cells which had been treated with paclitaxel (Fig. 8). This indicated that the presence of paclitaxel-treated cell lysates induced an inhibitory effect on the cleavage of the peptide by CPA in a dose dependent

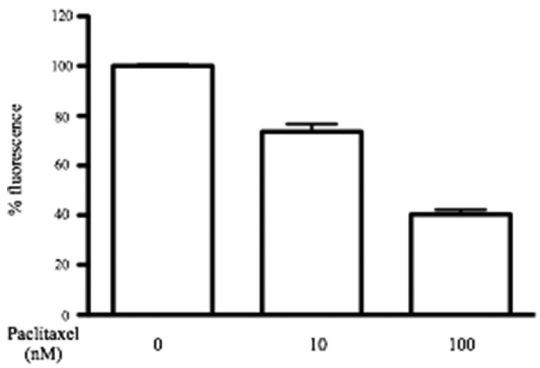

Fig. 7 Enzymatic cleavage of FRET peptide with supernatant from cell lysate. The FRET peptide was incubated with lysates harvested from cells that were incubated with paclitaxel at concentrations ranging from 0 to 100 nM.

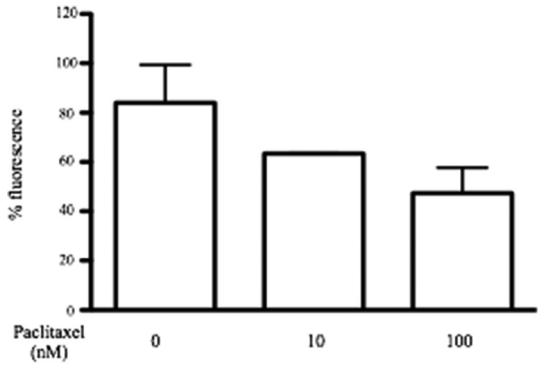

Fig. 8 FRET peptide cleavage competition assay. Cell lysate from cells incubated with varying concentrations of paclitaxel, or lysis buffer alone (LB), were pre-incubated for 1 hour with bovine CPA solution, followed by incubation with the FRET peptide for 1 hour.

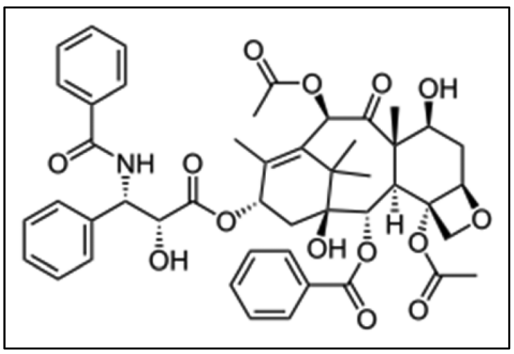

Fig. 9 Structure of the chemotherapy drug paclitaxel.

manner and confirmed the assumption of substrate competition between the biosensor and endogenous microtubules.

Discussion

Development of a biosensor for *in situ* treatment monitoring

Patient-related factors can dramatically alter drug pharmacokinetics (PK). These include organ function, expression and activity of metabolizing enzymes, drug resistance, body size, gender, age, drug concentration at the target site, number and functionality of the target receptors, concomitant disease and co-administration with other drugs.[10,18] It is often impossible at the onset of treatment to anticipate the response of any particular patient to a particular therapeutic. Therefore, monitoring of on-target activity of a drug can allow dose readjustment to obtain the desired effect.

Biosensors often utilize antibodies as the biomolecular recognition element. However, the widespread use of antibody-based immunoassays has been hindered by the difficulty in developing specific new antibodies to emerging targets.[19] In this study we have used a short peptide comprising the eight C-terminal residues of α-tubulin (Fig. 1 and 3). Compared to more complex protein-based affinity scaffolds, short unstructured peptides have several potential advantages that can be exploited for biosensor development: (1) peptides are more stable and resistant to degradation, (2) facile and inexpensive synthesis, and (3) they are more amenable to engineering at the molecular level.[20–22]

Paclitaxel is a diterpenoid centred around a bulky, complex, and fused taxane ring composed of a number of hydrophobic residues (Fig. 9), which makes it a highly lipophilic compound with a $\log P$ value (octanol-water partition coefficient) of approximately 4 and an aqueous solubility of less than 0.01 mg mL^{-1}.[23–25]

Poor water solubility is common for many anticancer drugs, and this hampers the ability of the drugs to be delivered *via* the intravenous route. Nanoparticle delivery can improve the bioavailability of poorly soluble drugs.[26] One particularly successful example of a strategy to overcome the solvent-related problems of paclitaxel, is that of Abraxane; a formulation of paclitaxel in which the drug is bonded to albumin as a delivery vehicle. (For a review of nanoparticle carriers for the delivery of paclitaxel, see Liu *et al.*, 2011).[27] MSNPs have previously been used for paclitaxel delivery *e.g.* paclitaxel was delivered to PANC-1 human cancer cells in MSNPs and was shown to be taken up through an energy-dependent endocytosis mechanism.[28]

The drug molecules are thought to be adsorbed both onto the surface of the silica nanoparticles and inside the pores by van der Waals forces and hydrogen bonds, which can easily be broken by contact with water; hence enabling detachment and release of the drug inside the cell.[29]

Our work confirms previous observations that paclitaxel can be delivered within a silica nanoparticle carrier.[30] Release experiments using the fluorescent BODIPY-FL Paclitaxel (Molecular Probes) showed that approximately 45% of the drug was released after 3 hours, and 87% after 24 hours (data not shown). This is similar to other studies showing release of drugs from MSNPs *e.g.* Morrison *et al.*, 2014,[14] DeMuth *et al.* 2011.[31] The sustained release over 24 hours would ensure better bioavailability of the drug in patients.

Other possible advantages of nanoparticle delivery of paclitaxel are overcoming multidrug resistance (MDR) in tumour cells,[32] a reduction in required doses administered,[33] and sustained bioavailability in target cancer tissue through enhanced permeability and retention.[34]

Paclitaxel and tubulin stability

The anti-mitotic drug paclitaxel is known to stabilize microtubules (MT), induce assembly of the microtubules and enhance the formation of MT bundles in cultured cells.[35] Upon stabilisation by paclitaxel, MTs can be detyrosinated to a noticeable extent, and this detyrosination occurs affects preformed MTs, rather than soluble tubulin.[36] The identity of the gene coding for the human tubulin-specific carboxypeptidase has been elusive and therefore initial experiments were performed using purified bovine pancreatic carboxypeptidase. All carboxypeptidases cleave the peptide bond of an amino acid residue at the

carboxy-terminal end of a peptide, but are classified as either type A, B, or C, depending upon their ability to cleave at certain amino acid residues.[37] In this study we used carboxypeptidase A (CPA) which has a strong preference for peptides containing aromatic amino acids, such as tyrosine. The bovine CPA cleaved the terminal residues from the peptide for both the linear peptide (Fig. 3) and the FRET peptide (Fig. 5) in a dose-dependent manner. Subsequently, cell lysates were prepared from SKOv3 cells that had been incubated with increasing concentrations of paclitaxel. An increase in detyrosination due to paclitaxel, as evidenced by increased Glu-tubulin (Fig. 4, insert) in the SKOv3 cells confirmed that paclitaxel induced microtubule stabilisation. It has been previously demonstrated that tubulin carboxypeptidase is associated with microtubules in living cells.[38] This is manifested by high levels of detyrosinated MTs since the carboxypeptidase has time to exert its activity before MT disassembly. Therefore, a high content of Glu-tubulin would be considered to be a marker of stable MTs; as found in paclitaxel incubated cells.[36,39–42] It is known that, *in vitro*, assembled tubulin is at least 2.5 fold better substrate than non-assembled tubulin for the tubulin carboxypeptidase activity.[43,44] Hence, the highly stabilised MTs in the paclitaxel-incubated cells would likely be associated with the enzyme, reducing the amount that is freely available in the cytoplasm (Scheme 1). This is consistent with our finding that increasing the concentration of paclitaxel, increased the number of stabilized MTs and consequently decreased the free enzyme that was available to exogenous peptide. The cleavage rate of the peptide would therefore act as a readout of the magnitude of paclitaxel-induced MT stabilisation.

The described biosensor would be highly relevant in the clinical setting where paclitaxel's bioavailability is known to be highly variable.[45–47] Furthermore, paclitaxel resistance can be mediated by structurally altered α- and β-tubulins, or an impaired ability to polymerize tubulin dimers into microtubules (*e.g.* high levels of the βIII isotype, a minor component of cellular β-tubulin that increases the dynamic instability of microtubules) leading to impaired microtubule assembly.[48–50] The biosensor could therefore indicate the stabilization state of the MTs and provide assist in establishing a diagnosis of paclitaxel resistance at the microtubule level.

Experimental

Peptide synthesis

FITC labelled peptide. The peptide sequence GEEEGEEYK was synthesized with the addition of a FITC group at the N-terminus, separated from the peptide by an aminohexanoic spacer; the C-terminus was amidated (Genscript, MW 1570). See also, Fig. 1b.

FRET pair peptide. The peptide sequence was synthesized with an N-terminal Abz fluorophore and a Dnp quencher group that was added to the free amine group of the lysine side-chain (see also Fig. 5).

Nanoparticle synthesis

The synthesis method was performed using the method of Hom *et al.*, 2010.[51] Briefly, 100 mg CTAB (99%; Aldrich,) was dissolved in 48 mL ddH_2O and 350 μL of 2 M NaOH and vigorously stirred in a round-bottom flask at 80 °C. After temperature stabilization, 500 μL TEOS (Aldrich) was added. After a further 2 h incubation, the nanoparticles were collected by centrifugation and washed twice with methanol. The CTAB surfactant was removed by overnight reflux in acidic methanol (20 mL methanol, 1 mL 37% hydrochloric acid) at 80 °C.

XRD

A light smearing of silicone grease was applied to a single crystal of silicon and the powder sample was sprinkled on to the crystal. The excess powder was tapped off and the crystal + powder were presented to the X-ray beam. XRD analysis was carried out using a fully automated Siemens D5000 powder diffractometer employing copper kα radiation (λ = 0.15406 nm)

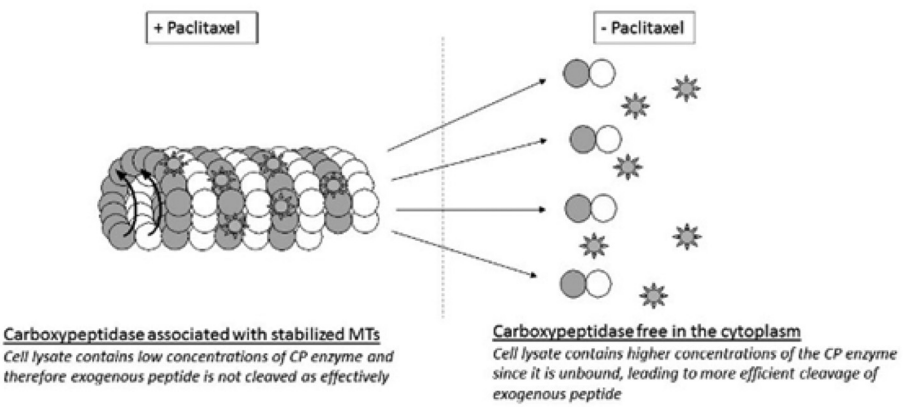

Scheme 1 Illustration to show the proposed mechanism behind the differences in cleavage rate of exogenous peptide with cell lysate. Within the cell, in the presence of taxol, the microtubules are stabilized and there is a greater association of carboxypeptidase (stars) with the protein resulting in less free enzyme in the lysate. (Tubulin dimers are shown as circles).

and a secondary monochromator. The samples were continuously spun during data collection and were scanned using a step size of 0.05° 2θ between the range of 5°–75° 2θ and a count time of 12 seconds per step. Power settings were 40 mA and 40 kV.

Nanoparticle loading with paclitaxel

MSNPs were suspended in dichloromethane at a concentration of 10 mg ml^{-1}. Paclitaxel was added to a final concentration of 120 μM, and the sample was sonicated in a sealed vessel in a water bath for 3 hours. The MSNPs were collected by centrifugation and the supernatant retained for analysis. The MSNPs were dried under vacuum to release trace dichloromethane.

The retained supernatants were analyzed by HPLC to determine the remaining concentrations of paclitaxel. The dichloromethane supernatant was taken to dryness and redissolved in 30% acetonitrile/70% water prior to analysis by high performance liquid chromatography (HPLC). HPLC was carried out on a Waters 2695 pump/autosampler with a Waters 2996 diode array detector. The column was a Phenomenex Luna C18, 3 μm, 150 × 2 mm, and the eluents were 10 mM formic acid (A) and acetonitrile (B). Taxol was separated using a gradient from 35–100% B over 11 min at a flow rate of 0.25 ml min^{-1}, and detected at 228 nm.

Release of paclitaxel from loaded nanoparticles in to PBS was similarly assessed by collecting supernatant, and adding methanol to the sample to ensure that the paclitaxel was not adsorbed on to sample tubes, prior to quantification by HPLC.

Conjugation of peptide to nanoparticle

The silica nanoparticles were aminated by the addition of 0.05% (v/v) 3-aminopropyl-trimethoxysilane (APTES) in water, for 1 h. The nanoparticles were then collected by centrifugation and washed twice with water. The nanoparticles were subsequently resuspended in 100 mM sodium carbonate buffer (pH 8.5). BS^3 linker was then added to the sample and incubated for 15 min. This linker contained an amine-reactive *N*-hydroxysulfosuccinimide (NHS) ester (Thermo Scientific Pierce) at each end of an 8-carbon spacer arm, and can therefore form stable amide bonds. The peptide was then added to the sample and the pH adjusted, and incubated at room temperature for 30 min with shaking. The nanoparticles were then collected by centrifugation and washed with PBS.

A calibration curve was generated to determine the relationship between the peptide concentration and fluorescence emission. Since a known quantity of MSNPs were used in the conjugation reaction, the amount of conjugated peptide can be deduced from the calibration curve.

Enzymatic cleavage

The peptide was cleaved using bovine pancreatic carboxypeptidase A (Sigma #C9268) which hydrolyzes peptide bonds of C-terminal residues with aromatic or aliphatic side chains. The enzyme is pre-treated with phenylmethylsulfonyl fluoride to eliminate trypsin and chymotrypsin activity.

Carboxypeptidase A was resuspended in 1 M NaCl at 10 units mL^{-1}. This solution was then diluted thirty-fold in buffer 2 (25 mM Tris-HCl, 500 mM NaCl; pH7.5).

Cell growth

Cell culture conditions. The ovarian cancer cell line SKOv3 was cultured in McCoy's 5A medium supplemented with 10% fetal bovine serum, 100 μg ml^{-1} streptomycin and 100 U ml^{-1} penicillin (Life Technologies, Paisley, UK). The cells were incubated at 37 °C in a humidified air atmosphere containing 5% CO_2.

Incubation with paclitaxel. SKOv3 cells were seeded on coverslips in 24-well plates at a density of 0.5 to 1.0 × 10^5 cell per well in 1.0 mL of complete McCoy's 5A medium. Cells were incubated overnight and grown to 50–80% confluence. Culture medium was removed and replaced with 0.5 mL of medium containing concentrations of paclitaxel ranging from 5 nM to 200 nM or paclitaxel-loaded nanoparticles. In control wells samples were either incubated with medium alone or unloaded nanoparticles. After treatment, cells were incubated for a further 18 h at 37 °C in 5% CO_2. Cells grown on the coverslips were then washed three times with PBS and fixed/permeabilized with ice-cold absolute ethanol followed by staining with Phospho-Histone H3 antibody (Cell signalling technology, Boston, USA). Stained cells were analysed under immunofluorescent microscope (Zeiss 780 inverted confocal).

Cell lysate preparation. SKOv3 cells were plated at a density of 3 × 10^5 cell per well in 6-well plate and cultured overnight. Culture medium was removed and replaced with complete McCoy's5A medium containing paclitaxel (10 nM to 500 nM). After 1 to 4 h incubation with paclitaxel the cells were detached by trypsinization, and transferred to 1.5 mL microcentrifuge tubes. Cells were centrifuged at 3000 rpm, and the cell pellets resuspended in 200 μl of cold lysis buffer (50 nM Tris-HCl; pH 7.4, 150 nM NaCl, 0.01% (v/v) Triton) with freshly added protease inhibitor (Invitrogen) and placed on ice for 30 min to ensure efficient lysis. Lysates were then centrifuged at 13 000 rpm for 15 min at 4 °C, and supernatants collected for the enzymatic cleavage assay.

Spectroscopy

Spectra were collected using a Cary Eclipse Fluorescence Spectrophotometer (Agilent). Samples were loaded into quartz cuvettes with a 1 cm light path (Hellma Analytics), and scanned with an excitation wavelength of 310 nm, with both excitation and emission slits set to 5 nm.

Western blotting

Western blotting was performed to assess levels of Glutubulin. Briefly, cell lysates were prepared from SKOv3 cells treated with various concentration of paclitaxel for 1 to 4 h. Protein concentration was determined for each lysate and equal amounts of protein (20–30 μg per well) were separated by SDS-PAGE for 2 h at 100 V, prior to protein transfer to nitrocellulose membrane. The membrane was blocked with 5% (w/v) milk in blocking buffer (1× TBS) at 4 °C overnight. Sub-

sequently the membrane was probed with Rabbit anti-detyrosinated tubulin (Glu-tubulin) antibody (Millipore), followed by the incubation with the secondary antibody, HRP conjugated anti-rabbit IgG (Sigma Aldrich). The signal was developed according to manufacturer's instructions (Pierce ECL Western blotting substrate).

Statistical tests

Samples were compared for significance used the student's *t*-test. A two-tailed distribution with unequal variance was assumed.

Conclusions

In this study we presented a novel system that comprises a nanoparticle carrier and a FRET-based peptide biosensor. We showed that the biosensor could be utilized as a measure of the on-target activity of paclitaxel. Some of the key mechanisms of poor response to paclitaxel are attributed to poor bioavailability and tubulin-mediated resistance mechanisms. Therefore, our novel delivery-biomarker combination could have important clinical implications. Future work will focus on further development and validation using *in vivo* preclinical models.

Acknowledgements

The authors would like to thank Cancer Research UK (Oxford Cancer Imaging Centre), Target Ovarian Cancer, the Oxford Biomedical Research Centre, the Medical Research Council, the National Institute of Health Research, and the Engineering and Physical Sciences Research Council for financial support. Begbroke Nano is acknowledged for access to materials characterisation equipment. We would also like to thank Boris Vojnovic, Iain Tullis, Davide Volpe, and Robert C Bast Jr for helpful discussions.

References

1 A. Ahmed, A. Mills, A. Ibrahim, J. Temple, C. Blenkiron, M. Vias, C. Massie, N. Iyer, A. McGeoch, R. Crawford, B. Nicke, J. Downward, C. Swanton, S. Bell, H. Earl, R. Laskey, C. Caldas and J. Brenton, *Cancer Cell*, 2007, **12**, 514–527.
2 A. Ahmed, X. Wang, Z. Lu, J. Goldsmith, X. Le, G. Grandjean, G. Bartholomeusz, B. Broom and R. Bast, *Cancer Res.*, 2011, **71**, 5806–5817.
3 S. Nakayama, Y. Torikoshi, T. Takahashi, T. Yoshida, T. Sudo, T. Matsushima, Y. Kawasaki, A. Katayama, K. Gohda, G. Hortobagyi, S. Noguchi, T. Sakai, H. Ishihara and N. Ueno, *Breast Cancer Res.*, 2009, **11**, 1.
4 S. Kumar, H. Mahdi, C. Bryant, J. Shah, G. Garg and A. Munkarah, *Int. J. Women's Health*, 2010, **2**, 411.
5 A. Sparreboom, C. Scripture, V. Trieu, P. Williams, T. De, A. Yang, B. Beals, W. Figg, M. Hawkins and N. Desai, *Clin. Cancer Res.*, 2005, **11**, 4136.
6 D. Nyman, K. Campbell, E. Hersh, K. Long, K. Richardson, V. Trieu, N. Desai, M. Hawkins and D. Von Hoff, *J. Clin. Oncol.*, 2005, **23**, 7785.
7 K. Yamada, N. Yamamoto, Y. Yamada, T. Mukohara, H. Minami and T. Tamura, *Jpn J. Clin. Oncol.*, 2010, **40**, 404.
8 E. Gardner, W. Dahut, C. Scripture, *et al.*, *Clin. Cancer Res.*, 2008, **14**, 4200.
9 T. Stinchcombe, M. Socinski, C. Walko, B. O'Neil, F. Collichio, A. Ivanova, H. Mu, M. Hawkins, R. Goldberg, C. Lindley and E. Dees, *Cancer Chemother. Pharmacol.*, 2007, **60**, 759.
10 Therapeutic drug monitoring and chemotherapeutics, Biomiga diagnostics.
11 D. Von Hoff, T. Ervin, F. Arena, E. Chiorean, J. Infante, M. Moore, T. Seay, S. Tjulandin, W. Ma, M. Saleh, M. Harris, M. Reni, S. Dowden, D. Laheru, N. Bahary, R. Ramanathan, J. Tabernero, M. Hidalgo, D. Goldstein, E. Van Cutsem, X. Wei, J. Iglesias and M. Renschler, *N. Engl. J. Med.*, 2013, **369**, 1691.
12 X. Huang, N. Young and H. Townley, *Nanomater. Nanotechnol.*, 2014, **4**, 2.
13 H. Hata, S. Saeki, T. Kimura, Y. Sugahara and K. Kuroda, *Chem. Mater.*, 1999, **11**, 1110.
14 R. Morrison, C. Gardiner, A. Evidente, R. Kiss and H. Townley, *Pharmaceutical Research*, 2014, **10**, 2904–2917.
15 M. Hendzel, Y. Wei, M. Mancini, *et al.*, *Chromosoma*, 1997, **106**, 348.
16 S. Huh, J. Wiench, B. Trewyn, *et al.*, *Chem. Commun.*, 2003, 2364.
17 H. Barra, C. Argarana and R. Caputto, *J. Neurochem.*, 1982, **38**, 112.
18 A. Roses, *Nature*, 2000, **405**, 857.
19 J. Kehoe and B. Kay, *Chem. Rev.*, 2005, **105**, 4056.
20 J. Dover, G. Hwang, E. Mullen, B. Prorok and S. Suh, *J. Microbiol. Methods*, 2009, **78**, 10.
21 S. Iqbal, M. Mayo, J. Bruno, B. Bronk, C. Batt, *et al.*, *Biosens. Bioelectron.*, 2000, **15**, 549.
22 J. Luong, K. Male and J. Glennon, *Biotechnol. Adv.*, 2008, **26**, 492.
23 R. Straubinger, in *Taxol: Science and Applications*, ed. M. Suffness, CRC Press, 1996, pp. 237–258.
24 P. Couvreur, P. Tulkens, M. Roland, A. Trouet and P. Speiser, *FEBS Lett.*, 1977, **84**, 323.
25 P. Couvreur, B. Kante, V. Lenaerts, V. Scailteur, M. Roland and P. Speiser, *J. Pharm. Sci.*, 1980, **69**, 199.
26 C. Fonseca, S. Simoes and R. Gaspar, *J. Controlled Release*, 2002, **83**, 273.
27 Y. Liu, B. Zhang and B. Yan, *Int. J. Mol. Sci.*, 2011, **12**, 4395.
28 J. Lu, M. Liong, S. Sherman, T. Xia, M. Kovochich, A. Nel, J. Zink and F. Tamanoi, *Nanobiotechnology*, 2007, **3**, 89.

29 L. Jia, J. Shen, Z. Liu, D. Zhang, Q. Zhang, G. Liu, D. Zheng and X. Tian, *Int. J. Pharm.*, 2013, **445**, 12–19.
30 H. Shen, C. Rodriguez-Aguayo, R. Xu, V. Gonzalez-Villasana, J. Mai, Y. Huang, G. Zhang, X. Guo, L. Bai, G. Qin, X. Deng, Q. Li, D. Erm, B. Aslan, X. Liu, J. Sakamoto, A. Chavez-Reyes, H. Han, A. Sood, M. Ferrari and G. Lopez-Berestein, *Clin. Cancer Res.*, 2013, **19**, 1806–1815.
31 P. DeMuth, M. Hurley, C. Wu, S. Galanie, M. R. Zachariah and P. DeShong, *Microporous Mesoporous Mater.*, 2011, **141**, 128–134.
32 L. Vigderman and E. Zubarev, *Adv. Drug Delivery Rev.*, 2013, **65**, 663.
33 D. Ayers and A. Nasti, *J. Drug Delivery*, 2012, 265691.
34 H. Maeda, H. Nakamura and J. Fang, *Adv. Drug Delivery Rev.*, 2013, **65**, 71.
35 P. Schiff and S. Horwitz, *Proc. Natl. Acad. Sci. U. S. A.*, 1980, **77**, 1561.
36 J. Wehland and K. Weber, *J. Cell Sci.*, 1987, **88**, 185.
37 J. Walker and J. Winder, *Protein Protocols Handbook*, ed. J. Walker, Humana Press, 1996, p. 967.
38 M. Contin, J. Sironi, H. Barra and C. Arce, *Biochem. J.*, 1999, **339**, 463.
39 M. Bre, T. Kreis and E. Karsenti, *J. Cell Biol.*, 1987, **105**, 1283.
40 T. Kreis, *EMBO J.*, 1987, **6**, 2577.
41 G. Gundersen, S. Khawaja and J. Bulinski, *J. Cell Biol.*, 1987, **105**, 251.
42 J. Bulinski and G. Gundersen, *Bioessays*, 1991, **13**, 285.
43 N. Kumar and M. Flavin, *J. Biol. Chem.*, 1982, **128**, 215.
44 C. Arce and H. Barra, *Biochem. J.*, 1985, **226**, 311.
45 W. Evans and M. Relling, *Clin. Pharmacokinet.*, 1989, **16**, 327.
46 G. Freyer, B. Ligneau, B. Tranchard, *et al.*, *Cancer Treat. Rev.*, 1997, **23**, 153.
47 E. Masson and W. Zamboni, *Clin. Pharmacokinet.*, 1997, **32**, 324.
48 M. Gonzalez-Garay, L. Chang, K. Blade, D. Menick and F. Cabral, *J. Biol. Chem.*, 1999, **274**, 23875.
49 P. Giannakakou, D. Sackett, Y. Kang, Z. Zhan, J. Buters, T. Fojo and M. Poruchynsky, *J. Biol. Chem.*, 1997, **272**, 17118.
50 M. Nicoletti, G. Valoti, P. Giannakakou, Z. Zhan, J. Kim, V. Lucchini, F. Landoni, J. Mayo, R. Giavazzi and T. Fojo, *Clin. Cancer Res.*, 2001, **7**, 2912.
51 C. Hom, J. Lu, M. Liong, H. Luo, X. Li, J. Zink and F. Tamanoi, *Small*, 2010, **6**, 1185.